A Numerical Study of a 3D Bioheat Transfer Problem with Different Spatial Heating *

Samir Karaa, † Jun Zhang, ‡
Laboratory for High Performance Scientific Computing and Computer Simulation,
Department of Computer Science, University of Kentucky,
773 Anderson Hall, Lexington, KY 40506–0046, USA

Fuqian Yang §
Department of Chemical & Materials Engineering, University of Kentucky,
161F Anderson Hall, Lexington, KY 40506–0046, USA

Abstract: We develop numerical methods for the computer simulation and modeling of a three dimensional heat transfer problem in biological bodies. The technique is intended for the temperature predications and parameter measurements in thermal medical practices and for the studies of thermomechanical interaction of biological bodies at high temperature.

We examine a mathematical model based on the classical well-known Pennes equation for heat transfer in biological bodies. A finite difference discretization scheme is used to discretize the governing partial differential equation. A preconditioned iterative solver is employed to solve the resulting sparse linear system at each time step. Numerical results are obtained to demonstrate the efficacy of the proposed numerical methods.

Key words: Bioheat transfer, Hyperthermia, Pennes equation, Preconditioning

1 Introduction

Modern clinical treatments and medicines such as cryosurgery, cryopreservation, cancer hyperthermia, and thermal disease diagnostics, etc., require the understanding of thermal life phenomena and temperature behavior in living tissues [2, 6]. Skin burns caused by exposing human body to heat in a flash fire or being in contact with hot substances are some of the most commonly encountered hazards in daily life and in industry [8]. Therefore, studying bioheat transfer in human body has been an interesting topic and is useful for effectively designing clinical thermal treatment equipments, for accurately evaluating skin burns, and for establishing thermal protections for various purposes.

Among the various models proposed to study the heat transfer in living tissues, the Pennes equation is the most widely used one [14]. It is based on the classical Fourier law, and has been greatly simplified after introducing the intuitive concept of blood perfusion (the blood flow rate per unit tissue volume), to study the bioheat transfer and assessment of skin burns.

Numerical techniques for solving 1D Pennes equation are discussed in [18]. Analytical solution of the 3D Pennes equation is presented in [10] using multidimensional Green function. Although this solution may be useful in some special cases, the complexity of multidimensional heat transfer problems in many practical situations suggests the application of numerical techniques. The objective of this paper is to present an implicit numerical solution of the Pennes' equation, which will be applied to study several selected typical bioheat transfer processes often encountered in cancer hyperthermia, laser surgery, and thermal parameter estimation.

*Technical Report No. 372-03, Department of Computer Science, University of Kentucky, Lexington, KY, 2003. This research work was supported in part by the U.S. National Science Foundation under grants CCR-9988165, CCR-0092532, ACR-0202934, and ACR-0234270, by the U.S. Department of Energy Office of Science under grant DE-FG02-02ER45961, by the Kentucky Science & Engineering Foundation under grant KSEF-02-264-RED-002, and by the Japanese Research Organization for Information Science & Technology.

†E-mail: samir@csr.uky.edu.
‡E-mail: jzhang@cs.uky.edu, URL: http://www.cs.uky.edu/~jzhang.
§fyang0@engr.uky.edu.

2 Heat Transfer Model

Figure 1 reflects a typical cancer hyperthermia where an apparatus is used to deposit a spatial heating for treating a tumor in the deep biological body while a surface cooling water is simultaneously adopted to prevent the surface healthy tissues from possible burn injury.

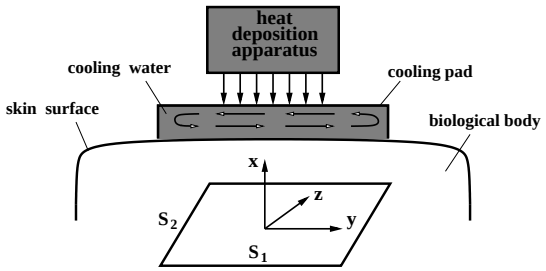

Figure 1: An illustration of a hyperthermia configuration.

The three dimensional Pennes equation corresponding to the practical situation depicted in Figure 1 is given by [10, 14]:

$$\rho C\frac{\partial T}{\partial t} = K\frac{\partial^2 T}{\partial^2 x}+K\frac{\partial^2 T}{\partial^2 y}+K\frac{\partial^2 T}{\partial^2 z} + W_b C_b(T_a - T) + Q_m + Q_r, \quad (1)$$

where ρ, C, and K are respectively the density, the specific heat and the thermal conductivity of the tissue. C_b is the specific heat of blood, W_b is the blood perfusion rate, T_a is the arterial temperature, and T represents the tissue temperature. Q_m and Q_r are respectively the volumetric metabolic heat and the external spatial heating. For simplicity, the constant thermal parameters are assumed but the random form for the external heating $Q_r(x, y, z; t)$ is reserved.

The boundary conditions (B.C.) corresponding to the configuration of Figure 1 are prescribed as follows [10]:

$$\text{B.C.} \quad \begin{cases} T = T_c \text{ at } x = 0; \quad K\dfrac{\partial T}{\partial x} = h_f(T - T_f) \text{ at } x = L, \\ K\dfrac{\partial T}{\partial y} = 0 \text{ at } y = 0; \quad K\dfrac{\partial T}{\partial y} = 0 \text{ at } y = s_1, \\ K\dfrac{\partial T}{\partial z} = 0 \text{ at } z = 0; \quad K\dfrac{\partial T}{\partial z} = 0 \text{ at } z = s_2, \end{cases} \quad (2)$$

where L is the depth of the tissue domain to be analyzed in the x direction. Here, the skin surface is defined at $x = L$ while the body core at $x = 0$. s_1 and s_2 are the widths of the tissue in the y- and z- direction respectively. The 3D computational domain is shown in Figure 2. Although more complex geometries can be considered, a particular regular geometry is selected for brevity. The other parameters are respectively: T_c the body core temperature which is regarded as constant, T_f the cooling fluid temperature, and h_f the convection coefficient. The reason for adopting adiabatic conditions in the two ends of the y- and z-direction is from the consideration that at the positions far from the beam center of the heat deposition apparatus, the temperature field is almost not affected by the external heating which generally has a strong decay in the y- and z-direction [10].

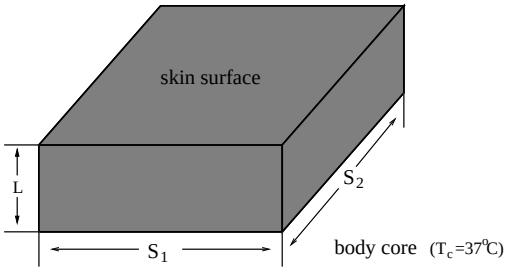

Figure 2: A 3D computational domain for numerical simulation.

By using the following transformations:

$$T = \theta + T_c + (T_c - T_f)\frac{x}{K/h_f - L},$$

and

$$Q^*(x, y, z, t) = Q_m + Q_r(x, y, z, t) + W_b C_b + \left[T_c + (T_c - T_f)\frac{x}{K/h_f - L}\right],$$

we rewrite the previous equation and the boundary conditions as

$$\frac{1}{\alpha}\frac{\partial \theta}{\partial t} = \frac{\partial^2 \theta}{\partial^2 x}+\frac{\partial^2 \theta}{\partial^2 y}+\frac{\partial^2 \theta}{\partial^2 z}-\frac{W_b C_b}{K}\theta+\frac{Q^*(x, y, z, t)}{K}, \quad (3)$$

and

$$\text{B.C.} \quad \begin{cases} \theta = 0 \text{ at } x = 0; \quad \dfrac{\partial \theta}{\partial x} = h_f\theta \text{ at } x = L, \\ \dfrac{\partial \theta}{\partial y} = 0 \text{ at } y = 0; \quad \dfrac{\partial \theta}{\partial y} = 0 \text{ at } y = s_1, \\ \dfrac{\partial \theta}{\partial z} = 0 \text{ at } z = 0; \quad \dfrac{\partial \theta}{\partial z} = 0 \text{ at } z = s_2, \end{cases} \quad (4)$$

respectively, where $\alpha = K/\rho C$ is the thermal diffusivity of tissue.

3 Numerical Scheme

Let n_x, n_y and n_z be the numbers of equally spaced grid points in the x-, y- and z-directions, respectively, and $\{x_{ijk} := (ih_x, jh_y, kh_z)\}$ the grid points in the computational domain, where $h_x = 1/n_x$, $h_y = 1/n_y$ and $h_z = 1/n_z$.

Let $\mathcal{L}$ be the elliptic operator defined by

$$\mathcal{L}\,\theta = \frac{\partial^2\theta}{\partial^2 x} + \frac{\partial^2\theta}{\partial^2 y} + \frac{\partial^2\theta}{\partial^2 z} - \frac{W_b C_b}{K}\theta.$$

We denote by $\mathcal{A}$ a finite difference approximation of $\mathcal{L}$ with p-th order accuracy, i.e.,

$$\mathcal{A}\,\theta \approx \mathcal{L}\,\theta + \mathcal{O}(h^p),$$

where $h = \max\{h_x, h_y, h_z\}$. Then the semi-discrete equation corresponding to Equation (3) reads

$$\frac{1}{\alpha}\frac{\partial\theta}{\partial t} = \mathcal{A}\,\theta + F,$$

where $F = Q^*/K$. To integrate in time, we use the two-level implicit time-stepping scheme

$$\frac{1}{\alpha}\frac{\theta^{n+1}-\theta^n}{\Delta t} = \mathcal{A}(\frac{1}{2}\theta^{n+1} + \frac{1}{2}\theta^n) + F^{n+1/2}, \qquad (5)$$

where Δt is the time step size, and θ^n is the discrete solution vector at time $t^n = n\Delta t$. This numerical scheme is known as the Crank-Nicolson scheme [3]. It yields a truncation error at the n-th time level

$$E = \mathcal{O}\left(\Delta t^2 + h^p\right).$$

In the matrix form we can represent (5) as:

$$\left(I - \frac{\alpha\Delta t}{2}\mathcal{A}\right)\theta^{n+1} = \left(I + \frac{\alpha\Delta t}{2}\mathcal{A}\right)\theta^n + \alpha\Delta t F^{n+1/2}. \qquad (6)$$

That is at time t^{n+1} the discrete solution is given by

$$\theta^{n+1} = \left(I - \frac{\alpha\Delta t}{2}\mathcal{A}\right)^{-1}\left(\left(I + \frac{\alpha\Delta t}{2}\mathcal{A}\right)\theta^n + \alpha\Delta t F^{n+1/2}\right).$$

4 Iterative Solution Strategy

In order to compute a numerical solution for the Pennes equation, the sparse linear system (6) is solved at each time step with the same coefficient matrix and a different right hand side. Thus, the total computational cost will be dominated by the way this linear system is solved. Direct solution methods based on Gaussian elimination are usually not practical for large size problems due to the excessive memory and computational (CPU) requirements. A common sparse linear system solution strategy in engineering society is to use either a direct band solver or alternating direction implicit (ADI) solution scheme. To solve the problem most efficiently, we propose to use a Krylov subspace method coupled with a robust preconditioner so that (6) can be solved in a few iterations at each time. We mainly focus on GMRES, a minimal residual algorithm based on the use of the Arnoldi process to construct an orthogonal basis of the Krylov subspace [15, 16]. In a full GMRES implementation the storage requirements grow quadratically with the number of iterations. Hence, in practice it is often necessary to use a restarted version, GMRES(m), where m indicates the selected dimension of the Krylov subspace. In this case, the algorithm is restarted after m iterations.

The convergence rate of GMRES can be speeded up by the technique of preconditioning. The basic idea of preconditioning is to replace the original system, namely $Ax = b$, by an equivalent system $M^{-1}Ax = M^{-1}b$, which will be easier to solve by an iterative method. The matrix M should be in general inexpensive to compute and easy to invert. The following algorithm describes GMRES(m) for solving $Ax = b$ with a preconditioner M.

ALGORITHM **1.** Left Preconditioned GMRES(m)

1. Choose x_0
2. Compute $r_0 = M^{-1}(b - Ax_0)$, $\beta = ||r_0||_2$, and $v_1 = r_0/\beta$
3. For $j = 1, \ldots, m$, Do
4. Compute $z = M^{-1}Av_j$
5. For $i = 1, \ldots, j$, Do
6. $h_{i,j} =, \ldots, j$, Do
7. $z = z - h_{i,j}v_i$
8. End For
9. Compute $h_{j+1,j} = ||z||_2$ and $v_{j+1} = z/h_{j+1,j}$
10. End For
11. Define $V_m = [v_1, \ldots, v_m]$, $\bar{H} = \{h_{i,j}\}_{1\le i\le j+1; 1\le j\le m}$
12. Compute y_m the minimizer of $||\beta_1 e_1 - \bar{H}y||_2$, and $x_m = x_0 + V_m y_m$
13. If convergence criterion is satisfied, then stop, otherwise set $x_0 = x_m$ and go to 1

Incomplete LU factorization has been one of the best known preconditioning techniques used to improve the convergence of GMRES [13]. The basic idea of the ILU factorization is to preserve the sparsity in the L and U factors by neglecting most, or even all, the fill-in terms during the elimination process. Of course the product matrix LU is then only an approximation of the coefficient matrix. More discussions on different Krylov subspace methods and various type of incomplete LU factorization preconditioning techniques can be found in [15].

5 Numerical Results

We solve the 3D problem (3)-(4) with the numerical discretization scheme described in Section 2. We choose a second order central difference scheme in space. The typical values for tissue properties and other parameters are applied as given in [7], $\rho = 1000\,\mathrm{kg/m^3}$, $C = C_b = 4000^o\mathrm{CJ/kg}$, $T_a = T_c = 37^o\,\mathrm{C}$, $K = 0.5^o\,\mathrm{CW/m}$,

$W_b = 0.5\,\mathrm{kg/m^3s}$, $Q_m = 420\,\mathrm{W/m^3}$, $h = 10^o\mathrm{W/m^2}$. The surrounding fluid temperature was chosen as $T_f = 25^o$ C. As demonstrated in many works [11, 17], the interior tissue temperature usually tends to a constant within a short distance such as 2-3 cm. Therefore $L = 3$ cm was used in this study. For some particular issues, such as deeper heating, or more intense sources of heat, the distance between skin surface and the body core will exceed this depth. In this case, new bounded core large enough to neglect the influence of the surface heating should be incorporated into the calculations.

Although any heating style for Q_r can be dealt with by the present computation, only the most popular and simple specific absorption rate (SAR) expression for Q_r will be particularly analyzed. For the plane wave heating of laser or microwave, the heat absorption in the muscle tissue can simply be approximated by Beer's law as [9, 12]:

$$Q_r(x, y, z, t) = \eta P_0(t) \exp[-\eta(L - x)],$$

where $P_0(t)$ is the time-depending heating power on skin surface, and η the scattering coefficient.

Since the heating power and the scattering coefficient may vary from one heating apparatus to another, it is of great importance to study the influence of these parameters upon the behavior of the tissue temperature. Such study is expected to be very useful in a large variety of bio-thermal practices.

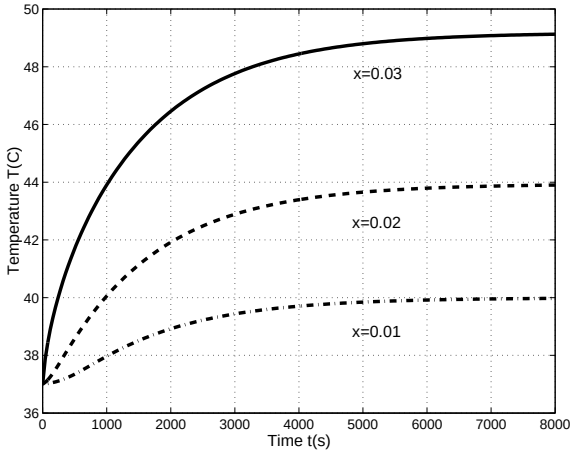

Figure 3: Transient temperature at 3 different locations with constant heating ($\eta = 200$).

Effect of power heating. Figures 3 and 4 show the transient temperatures at three different locations of the skin when the biological body is subject to two different spatial heating. Figure 3 depicts the case of constant heating, and Figure 4 the case of sinusoidal heating. The former one reflects the situation where the human skin is heated by a laser [5], while the later case can be found in the perfusion estimation [1].

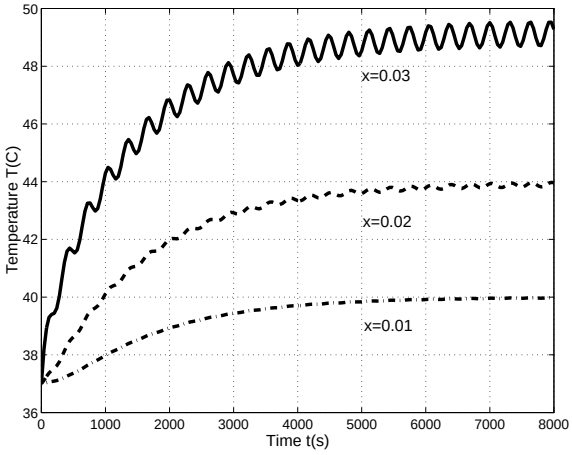

Figure 4: Transient temperature at 3 different locations, with sinusoidal heating ($\eta = 200$).

Obviously, in both cases, the highest temperature increase occurs at the surface while smaller temperature increase occurs inside the tissue due to the decay of the spatial heating. We also remark that as the time becomes long enough, the temperature approaches a steady-state value. In this calculations we assumed that the initial temperature at $t = 0$ inside the skin is uniform and equal to the body core temperature, i.e., $T_0(x, y, z, t) = 37^o$ C. Since the heat transfer process is very slow, a time step $\Delta t = 20s$ was selected. This shows the advantage of using an implicit unconditionally stable scheme.

Effect of the scattering coefficient. Figures 5 and 6 show the effects of the scattering coefficient on the temperature transients at the skin surface. Clearly, the larger the scattering coefficient, the higher the temperature increases. Particularly, in Figure 6, one can still find that the larger the scattering coefficient, the higher amplitudes of the temperature oscillation. Here the initial temperature inside the skin is assumed to be constant and equal to the body core temperature.

Since different heating apparatus such as laser or microwave may have different power and scattering coefficient, calculations as performed are expected to be useful for the heating-dose planning during a hyperthermia treatment or parameter estimation. For example, performances of different heating apparatus with specific power and decay coefficient can be evaluated using the present computation to predict the temperature response thus induced in the tissue.

Figure 7 shows the transient temperature distributions

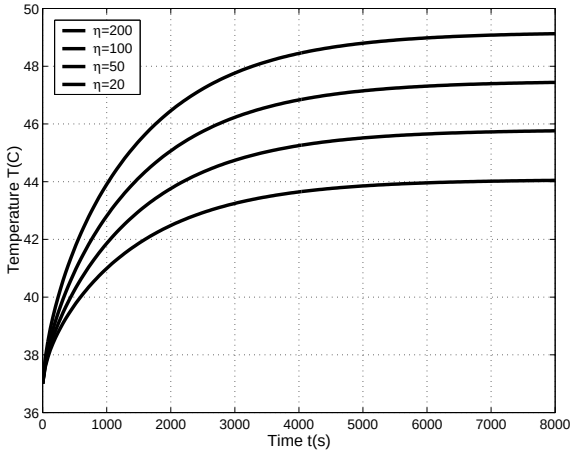

Figure 5: Skin surface transient temperature with constant heating for different values of η.

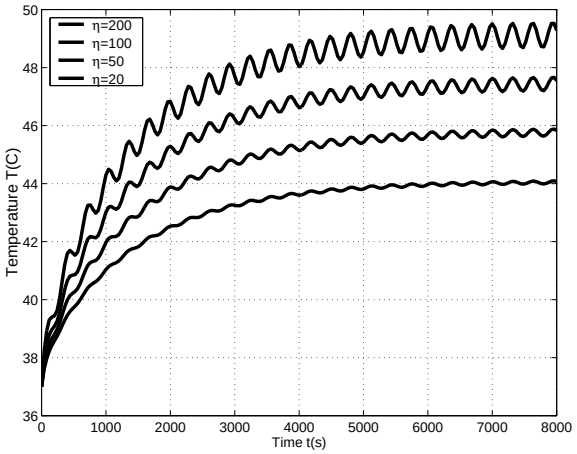

Figure 6: Skin surface transient temperature with sinusoidal heating for different values of η.

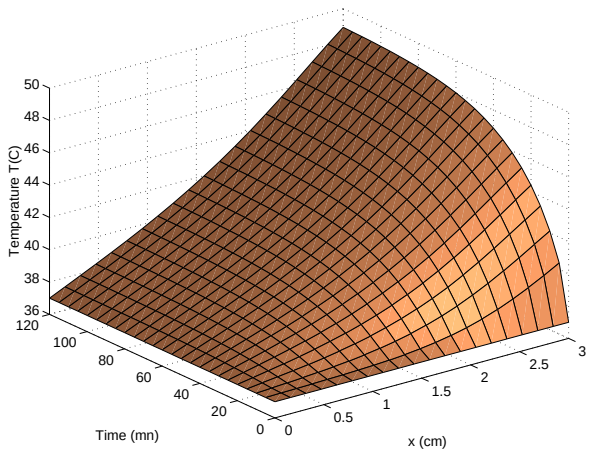

Figure 7: Temperature distribution along a specified x-direction with T_0 being constant.

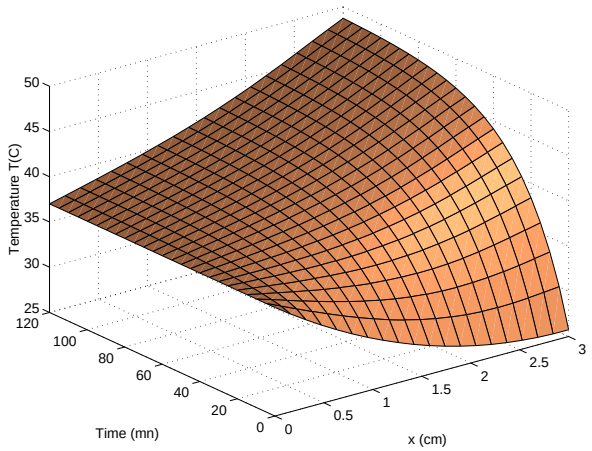

Figure 8: Temperature distribution along a specified x-direction with T_0 being variable.

along a specified x-direction at several time intervals. Since the temperature at time $t = 0$ is assumed to be constant, the highest temperature occurs at the skin surface at all times. Figure 8 shows a different situation where the initial temperature is chosen of the form $T_0(x, y, z, t) = ax^2 + bx + c$, with $T_0 = 37^o$C at $x = 0$ and $T_0 = 26^o$C at the sling surface ($x = L$). At the early stage of the heating, the tissue temperature decreases from the body core to the skin surface. However, it will gradually be improved due to the spatial heating until it reaches a steady state.

Point-heating sources. In many thermal medical practices, internal heating is adopted for treating tumor in the deep tissue by selectively attack the regional tumor with high temperature level. In this part we investigate the temperature response near the tumor sites when point-heating is adopted. Practical examples of point heating can be found in clinical treatments where heat is deposited through inserting a conducting heating probe in the deep tumor site. In contrast to the previous heating style where the heat flux decays exponentially with the distance from the skin surface, here the point-heating source to be studied is of the form:

$$Q_r(x, y, z, t) = P_1(t)\delta(x - x_0)\delta(x - y_0)\delta(x - z_0),$$

where, P_1 is the point-heating power, δ is the Dirac function, and (x_0, y_0, z_0) the position of point-heating source.

The numerical results are given in Figures 9 and 10. They depict the steady state temperature distribution in the biological body heated by one and three point-heating sources, respectively. The strength of each

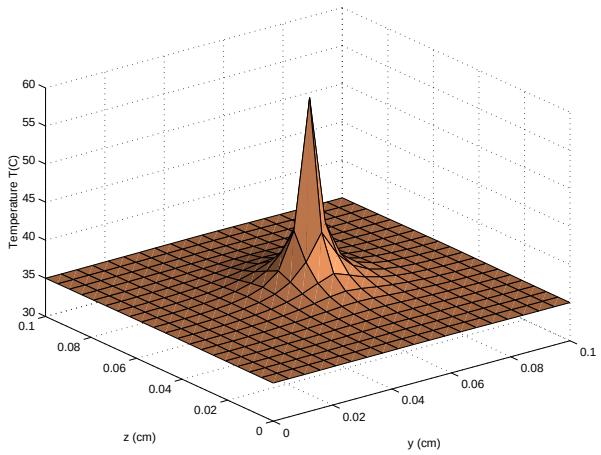

Figure 9: Steady state temperature distribution at one profile ($x = 0.015$ m), with one point-heating source.

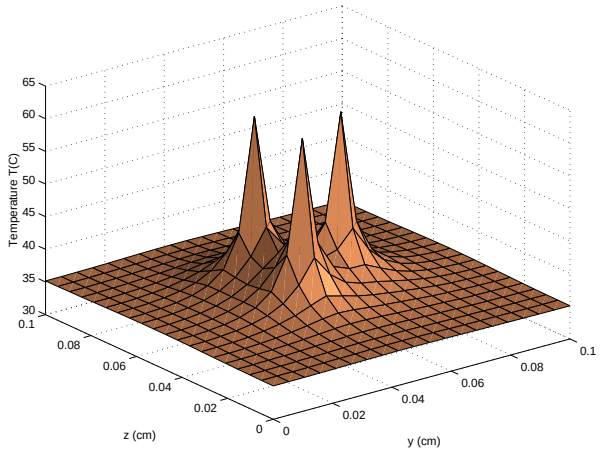

Figure 10: Steady state temperature distribution at one profile ($x = 0.015$ m), with three point-heating sources.

point-heating source is $P_1(t) = 4.8 \times 10^6$, while the cooling medium temperature at the skin surface is set at 16^oC. In Figure 9, the single heating source is placed at position $(0.015\,\text{m}, 0.05\,\text{m}, 0.05\,\text{m})$, and in Figure 10, the three point-heating sources are fixed at positions $(0.015\,\text{m}, 0.042\,\text{m}, 0.042\,\text{m})$, $(0.015\,\text{m}, 0.042\,\text{m}, 0.063\,\text{m})$, and $(0.015\,\text{m}, 0.063\,\text{m}, 0.052\,\text{m})$, respectively.

As expected, the results show that the maximum steady temperature of the tissue occurs at the positions of point-heating sources. We also observe that the temperature of the tissues around the point-heating sources is fairly below 37^oC on the whole. This has a great benefit for hyperthermia treatment, since the temperature at the diseased tissue sites can be selectively controlled, while the temperature of the healthy tissues surrounding the diseased area stays below the safe threshold. This is one of the most attractive features why internal heating is frequently used to thermally kill tumors in the deep tissue, although it may cause some mechanical injuries. We mention that our numerical results agree very well with the experiments conducted in [4], where similar bioheat transfer processes with spatial and transient heatings on skin and inside biological bodies are studied.

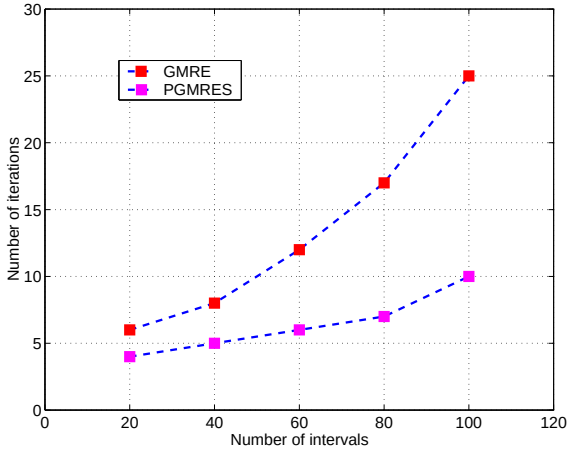

Figure 11: Comparison of the number of iterations between GMRES and preconditioned GMRES using ILU(0) for solving the linear system with different numbers of grid points.

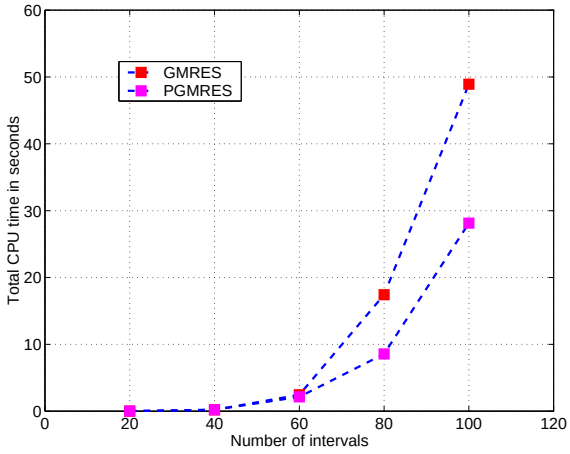

Figure 12: Comparison of the total CPU time between GMRES and preconditioned GMRES using ILU(0) for solving the linear system with different numbers of grid points.

We finally computed a few simulations using different values of N, where $N = n_x = n_y = n_z$. That is we choose the same number of grid points in each direction. Figures 11 and 12 compare unpreconditioned GMRES(10)

with preconditioned GMRES(10) (PGMRES) using the ILU(0) preconditioner with respect to the number of iterations (Figure 11) and the total CPU time in seconds (Figure 12) for different values of N. As is expected, PGMRES took less iterations to converge than GMRES did. However the CPU time in each case is almost the same when $N \leq 60$. For large size linear systems ($N \geq 60$), PGMRES converges much faster than GMRES which demonstrates the usefulness of the ILU preconditioner.

6 Concluding Remarks

We presented a numerical study of a 3D bioheat transfer equation with different heating styles. An implicit unconditionally stable numerical scheme, which has the advantage of allowing large time step size, is used and a preconditioned Krylov subspace iterative method is selected to solve the resulting sparse linear systems. The computations presented in this work can be used to predict the evolution of the temperature within the tissue during many bioheat transfer processes. For example, performances of different heating apparatus with specific power and decay coefficient can be evaluated using the present computation to predict the temperature response induced in the tissue.

References

[1] G. T. Anderson and G. Burnside, A non-invasive technique to measure perfusion using a focused ultrasound heating source and a tissue surface temperature measurement, in *Proc. Advance in Measuring and Computing Temperatures in Biomedicine*, **147**, 31–35, (1990).

[2] J. C. Chato, *Fundamentals of Bioheat Transfer*, Springer-Verlag, Berlin, (1989).

[3] J. Crank and P. Nicolson, A practical method for numerical evaluation of solution of partial differential equations of the heat-conduction type, *Proc. Cambridge Philos. Soc.*, **43**, 50–67, (1947).

[4] Deng Z. S. and Liu J., Analytical study on bioheat transfer problems with spatial or transient heating on skin surface or inside biological bodies, *ASME J. Biomechan. Eng.*, **124**, 638–649, (2002).

[5] K. R. Diller, Modeling of bioheat transfer processes at high and low temperatures, *Adv. Heat Transfer*, **22**, 157–167, (1992).

[6] M. Gautherie, *Clinical Thermology*, Springer-Verlag, Heidelberg, Vol. 1-4, (1990).

[7] K. R. Holmes, Biological structures and heat transfer, in *Allerton Workshop on the Future of Biothermal Engineering*, (1997).

[8] K. R. Killer and L. J. Hayes, Analysis of tissue injury by burning: comparison of in situ and skin flap models, *Int. J. Heat Mass Transfer*, **34**, 1393–1406, (1991).

[9] J. B. Leonard, K. B. Foster, and T. W. Athey, Thermal properties of tissue equivalent phantom materials, *IEEE Trans. Biomed. Eng.*, **31**, 533–536, (1984).

[10] J. Liu, Uncertainty analysis for temperature prediction of biological bodies subject to randomly spatial heating, *J. Biomechan.*, **34**, 1637–1642, (2001).

[11] J. Liu and L. X. Xu, Estimation of blood perfusion using phase shift in temperature response to sinusoidal heating at skin surface, *IEEE Trans. Biomed. Eng.*, **46**, 1037–1043, (2001).

[12] P. Liu and G. Liu, *Action Mechanisms of Laser Biology*, Science Press, Beijing, pp. 127–177, 1989, (in Chinese).

[13] J. A. Meijerink and H. A. van der Vorst, An iterative solution method for linear systems of which the coefficient matrix is a symmetric M-matrix, *Math. Comput.*, **31**, 148–162, (1977).

[14] H. H. Pennes, Analysis of tissue and arterial blood temperature in the resting human forearm, *J. Appl. Physiol.*, **1**, 93–122, (1948).

[15] Y. Saad, *Iterative Methods for Sparse Linear Systems*, PWS Publishing, New York, NY, (1996).

[16] Y. Saad and M. H. Schultz, GMRES: a generalized minimal residual algorithm for solving nonsymmetric linear systems, *SIAM J. Sci. Stat. Comput.*, **7**, 856–869, (1986).

[17] S. Weinbaum, L. M. Jiji, and D. E. Lemons, Theory and experiment for the effect of vascular microstructure on surface tissue heat transfer part I: anatomical foundation and model conceptualization, *ASME J. Biomech. Eng.*, **106**, 321–330, (2001).

[18] J. J. Zhao, J. Zhang, N. Kang, and F. Yang, A two level finite difference scheme for one dimensional Pennes' bioheat equation, Technical Report No. 354-02, Department of Computer Science, University of Kentucky, Lexington, KY, 2002.